# *On an electrothermomechanical model arising in steel heat treating*

José Manuel Díaz Moreno

*Departamento de Matemáticas, Universidad de Cádiz, Spain*

Concepción García Vázquez

*Departamento de Matemáticas, Universidad de Cádiz, Spain*

María Teresa González Montesinos

*Departamento de Matemática Aplicada I, Universidad de Sevilla, Spain*

Francisco Ortegón Gallego

*Departamento de Matemáticas, Universidad de Cádiz, Spain*

**Abstract**

Steel heat treating is very important for many industrial purposes. In this paper, we describe a mathematical model for the heating-cooling process of a steel workpiece leading to the desired hardness. The resulting model consists of a strongly coupled nonlinear system of PDEs/ODEs. A simpler version of this model is used for the numerical simulation of the hardening process of a car steering rack.

## 1 Introduction

Steel is an alloy of iron and carbon. Steel used for industrial purposes, has a carbon content up to about 2 wt%. Other alloying elements may be present, such as Cr and V in tools steels, or Si, Mn, Ni and Cr in stainless steels. Most structural components in mechanical engineering are made of steel. Certain of these components, such as toothed wheels, bevel gears, pinions and so on, engaged each others in order to transmit some kind of (rotational or longitudinal) movement. As a result the contact surfaces of these components are particularly stressed. The goal of heat treating of steel is to attain a satisfactory hardness.

Prior to heat treating, steel is a soft and ductile material. Without a hardening treatment, and due to the surface stresses, the gear teeth will soon get damaged and they will no longer engage correctly.

In this work we are interested in the mathematical description and the numerical simulation of the hardening procedure of a car steering rack (see Figure 1). This particular situation is one of the major concerns in the automotive industry. In this case, the goal is to increase the hardness of the steel along the tooth line and at the same time maintain the rest of the workpiece soft and ductile in order to reduce fatigue.

Figure 1: Car steering rack.

Solid steel may be present at different phases, namely austenite, martensite, bainite, pearlite and ferrite. The phase diagram of steel is shown in Figure 2. For a given wt% of carbon content up to 2.11, all steel phases are transformed into austenite provided the temperature has been raised up to a certain range. The minimum austenization temperature (727°) is attained for a carbon content of 0.77 wt% (eutectoid steel). Upon cooling, the austenite is transformed back into the other phases (see Figure 3), but its distribution depends strongly on the cooling strategy ([4, 12]).

Martensite is the hardest constituent in steel, but at the same time is the most brittle, whereas pearlite is the softest and more ductile phase. Martensite derives from austenite and can be obtained only if the cooling rate is high enough. Otherwise, the rest of the steel phases will appear. Figure 4 shows a time-temperature transformation diagram (TTT) of a given steel. Solid black curves indicate the beginning and the end of a transformation to another phase. Depending on the temperature history of $P_1$ to $P_4$, different phases are obtained.

The hardness of the martensite phase is due to a strong supersaturation of carbon atoms in the iron lattice and to a high density of crystal defects. From the industrial standpoint, heat treating of steel has a collateral problem: hardening is usually accompanied by distortions of the workpiece. The main reasons of these distortions are due to (1) thermal strains, since steel phases undergo different volumetric changes during the heating and cooling processes, and (2) experiments with steel workpieces under applied loading show an irreversible deformation even when the equivalent stress corresponding to the load is in the elastic range. This effect is called transformation induced plasticity.

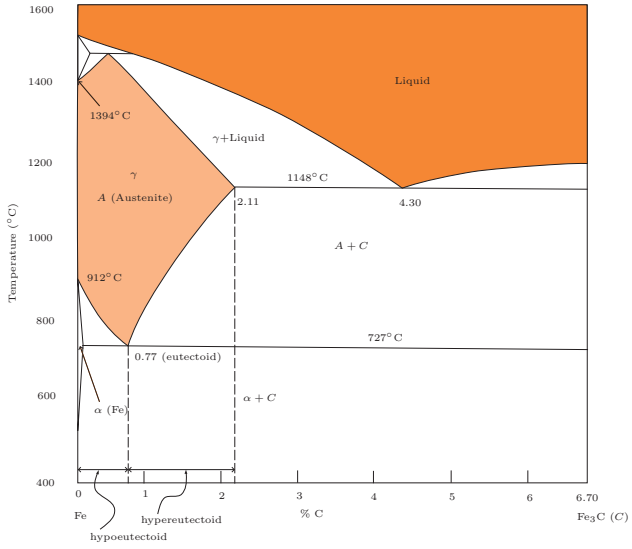


Figure 2: Phase diagram of steel. Austenite constituent is stable at a high temperature range.

The heating stage is accomplished by an induction-conduction procedure. This technique has been successfully used in industry since the last century. During a time interval, a high frequency current passes through a coil generating an alternating magnetic field which induces eddy currents in the workpiece, which is placed close to the coil. The eddy currents dissipate energy in the workpiece producing the necessary heating.

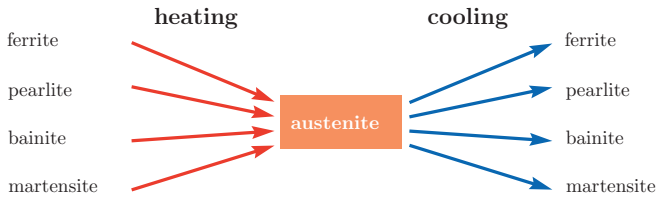


Figure 3: Microconstituents of steel. Upon heating, all phases are transformed into austenite, which is transformed back to the other phases during the cooling process. The distribution of the new phases depends strongly on the cooling strategy. A high cooling rate transforms austenite into martensite. A slow cooling rate transforms austenite into pearlite.

## 2 Mathematical modeling

We consider the setting corresponding to Figure 5. The domain $\Omega^{\mathrm{c}}$ represents the inductor (made of copper) whereas $\Omega^{\mathrm{s}}$ stands for the steel workpiece to be hardened. Here, the coil is the domain $\Omega = \Omega^{\mathrm{s}} \cup \Omega^{\mathrm{c}} \cup S_0$. In this way, the workpiece itself takes part of the coil.

In order to describe the heating-cooling process, we will distinguish two subintervals forming a partition of $[0, T]$, namely $[0, T] = [0, T_{\mathrm{h}}) \cup [T_h, T_{\mathrm{c}}]$, $T_{\mathrm{c}} > T_{\mathrm{h}} > 0$. The first one $[0, T_{\mathrm{h}})$ corresponds to the heating process. All along this time interval, a high frequency electric current is supplied through the conductor which in its turn induces a magnetic field. The combined effect of both conduction and induction gives rise to a production term in the energy balance equation (2.14), namely $b(\theta)|\boldsymbol{\mathcal{A}}_t + \nabla\phi|^2$. This is Joule's heating which is the principal term in heat production. In our model, we will only consider three steel phase fractions, namely austenite ($a$), martensite ($m$), and the rest of phases ($r$). In this way, we have $a + m + r = 1$ and $0 \leq a, m, r \leq 1$ in $\Omega^{\mathrm{s}} \times [0, T]$. At the initial time we have $r(0) = 1$ in $\Omega^{\mathrm{s}}$. Upon heating only austenite can be obtained. In particular $m = 0$ in $\Omega^{\mathrm{s}} \times [0, T_{\mathrm{h}}]$ and the transformation to austenite is derived at the expense of the other phase fractions ($r$).

At the instant $t = T_{\mathrm{h}}$, the current is switched off and during the time interval $[T_h, T_{\mathrm{c}}]$ the workpiece is severely cooled down by means of aqua-quenching.

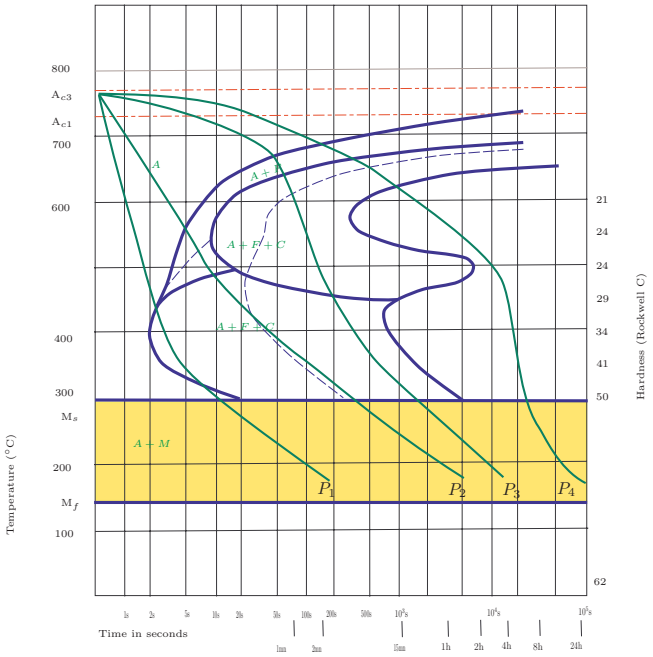


Figure 4: Temperature-Time transformation diagram (TTT). This isothermal transformation diagram (solid black lines) shows what happens when an austenized steel is held at a constant temperature. Continuous-cooling transformation diagram (CCT) is a non-isothermal transformation diagram describing the decomposition of austenite according to the corresponding temperature history curves (solid green curves). Generally, the CCT diagram (which is not represented here) have the same shape that the corresponding TTT diagram, but the transformation curves are shifted to right.

The cooling rate of $P_1$ is high enough so that it will be transformed into martensite. The cooling rate of $P_2$ is still high, but not enough. $P_2$ will transform into a mixture of martensite and nodular pearlite. $P_3$ will transform into fine pearlite. The point $P_4$ cools down very slowly and will transform into pearlite.

$A_{c1} = 727°C$ is the temperature at which austenite begins to form during the heating stage. The subscript $c$ comes from the French *chauffant*.

$A_{c3}$ is the temperature at which transformation of ferrite to austenite is completed during heating (for a hypoeutectoid steel, this value corresponds to the lower boundary of the austenite region in the phase diagram (Figure 2).

$M_s$ is the temperature at which transformation of austenite to martensite starts during the cooling stage.

$M_f$ is the temperature at which transformation of austenite to martensite finishes during cooling.

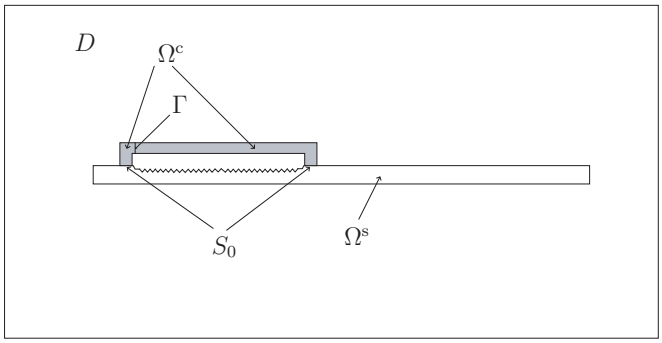


Figure 5: Domains $D$, $\Omega = \Omega^{\rm s} \cup \Omega^{\rm c} \cup S_0$ and the interface $\Gamma \subset \Omega^{\rm c}$. The inductor $\Omega^{\rm c}$ is made of copper. The workpiece contains a toothed part to be hardened by means of the heating-cooling process described below. It is made of a hypoeutectoid steel.

## The heating model

The current passing through the set of conductors $\Omega = \Omega^{\rm c} \cup \Omega^{\rm s} \cup S_0$ is modeled with the aid of an auxiliary smooth surface $\Gamma \subset \Omega^{\rm c}$ cutting the inductor $\Omega^{\rm c}$ into two parts, each one of them having a surface contact over the boundary of the workpiece $\Omega^{\rm s}$ (see Figure 5). The heating model involves the following unknowns: the electric potential, $\phi$; the magnetic vector potential, $\boldsymbol{\mathcal{A}} = (\boldsymbol{\mathcal{A}}_1, \boldsymbol{\mathcal{A}}_2, \boldsymbol{\mathcal{A}}_3)$; the stress tensor, $\boldsymbol{\sigma} = (\boldsymbol{\sigma}_{ij})_{1\le i,j\le 3}$, $\boldsymbol{\sigma}_{ij} = \boldsymbol{\sigma}_{ji}$ for all $1 \le i, j \le 3$; the displacement field $u = (u_1, u_2, u_3)$; the austenite phase fraction, $a$; and the temperature, $\theta$. Among them, only $\boldsymbol{\mathcal{A}}$ is defined in the domain $D$ containing the set of conductors $\Omega$. On the other hand, since the inductor and the workpiece are in close contact, both $\phi$ and $\theta$ are defined in $\Omega$. Since phase transitions only occur in the workpiece, we may neglect deformations in $\Omega^{\rm c}$. This implies that $\boldsymbol{\sigma}$, $u$ and $a$ are only defined in the workpiece $\Omega^{\rm s}$. The heating model reads as follows ([3, 9, 10, 7]):

$$\nabla \cdot (b(\theta)\nabla\phi) = 0 \quad \text{in } \Omega_{T_{\rm h}} = \Omega \times (0, T_{\rm h}), \tag{2.1}$$

$$\frac{\partial \phi}{\partial n} = 0 \quad \text{on } \partial\Omega \times (0, T_{\rm h}), \tag{2.2}$$

$$\left[ b(\theta) \frac{\partial \phi}{\partial n} \right]_{\Gamma} = j_S \quad \text{on } \Gamma \times (0, T_{\rm h}), \tag{2.3}$$

$$b_0(\theta)\boldsymbol{\mathcal{A}}_t + \nabla \times \left(\frac{1}{\mu}\nabla \times \boldsymbol{\mathcal{A}}\right) - \delta\nabla(\nabla \cdot \boldsymbol{\mathcal{A}}) = -b_0(\theta)\nabla\phi \quad \text{in } D \times (0, T_{\rm h}), \tag{2.4}$$

$$\boldsymbol{\mathcal{A}} = 0 \quad \text{on } \partial D \times (0, T_{\rm h}), \tag{2.5}$$

$$\boldsymbol{\mathcal{A}}(0) = \boldsymbol{\mathcal{A}}_0 \quad \text{in } \Omega, \tag{2.6}$$

$$-\nabla \cdot \boldsymbol{\sigma} = F \quad \text{in } \Omega^{\rm s} \times (0, T_{\rm h}), \tag{2.7}$$

$$\boldsymbol{\sigma} = \boldsymbol{K}\left(\boldsymbol{\varepsilon}(u) - A_1(a, m, \theta)\boldsymbol{I} - \int_0^t \gamma(a, m, a_t, m_t, \theta)\boldsymbol{S}\,\mathrm{d}\tau\right), \tag{2.8}$$

$$u = 0 \quad \text{on } \Gamma_0 \times (0, T_{\rm h}), \tag{2.9}$$

$$\boldsymbol{\sigma}\, n = 0 \quad \text{on } \Gamma_1 \times (0, T_{\rm h}), \tag{2.10}$$

$$a_t = \frac{1}{\tau_a(\theta)}(a_{\rm eq}(\theta) - a)\mathcal{H}(\theta - A_s) \quad \text{in } \Omega^{\rm s} \times (0, T_{\rm h}), \tag{2.11}$$

$$a(0) = 0 \quad \text{in } \Omega^{\rm s}, \tag{2.12}$$

$$\begin{aligned}\alpha(\theta, a, m, \boldsymbol{\sigma})\theta_t - \nabla \cdot (\kappa(\theta)\nabla\theta) + 3\bar{\kappa}q(a, m)\theta\,(\nabla \cdot u_t - 3A_2(a_t, m_t, \theta)) = \\ = b(\theta)|\boldsymbol{\mathcal{A}}_t + \nabla\phi|^2 - \rho L_a a_t + A_2(a_t, m_t, \theta)\,\mathrm{tr}\,\boldsymbol{\sigma} + \gamma(a, m, a_t, m_t, \theta)|\boldsymbol{S}|^2 \ \text{ in } \Omega_{T_{\rm h}},\end{aligned} \tag{2.13}$$

$$\frac{\partial\theta}{\partial n} = 0 \quad \text{on } \partial\Omega \times (0, T_{\rm h}), \tag{2.14}$$

$$\theta(0) = \theta_0 \quad \text{in } \Omega. \tag{2.15}$$

Here, $b(\theta)$ is the electrical conductivity (by $b(\theta)$ we mean the function $(x,t) \mapsto b(x,\theta(x,t))$, and also for $\kappa(\theta)$, etc.); $[\,\cdot\,]_\Gamma$ stands for the jump across the inner surface $\Gamma$; $j_S$ represents the external source current density. The domain $D$ containing the set of conductors is taken big enough so that the magnetic vector potential $\boldsymbol{\mathcal{A}}$ vanishes on its boundary $\partial D$. Since both $\boldsymbol{\sigma}$ and $a$ are only defined in $\Omega^{\rm s}$, when they appear in a term referred in $\Omega$, we mean that this term vanishes outside $\Omega^{\rm s}$ (for instance, $-\rho L_a a_t$ appearing in (2.13)); $b_0(x,s) = b(x,s)$ if $x \in \Omega$, $b_0(x,s) = 0$ elsewhere; $\mu = \mu(x)$ is the magnetic permeability; $\delta > 0$ is a small constant; $F$ is a given external force (usually $F = 0$); $\boldsymbol{K} = \boldsymbol{K}_{ijkl}$, $1 \le i,j,k,l \le 3$ is the stiffness tensor. Steel can be considered as an isotropic and homogenous material so that

$$\boldsymbol{K}_{ijkl} = \bar{\lambda}\delta_{ij}\delta_{kl} + \bar{\mu}(\delta_{ik}\delta_{jl} + \delta_{il}\delta_{jk}), \ \text{for all } i,j,k,l \in \{1,2,3\}$$

where $\bar{\lambda} \ge 0$ and $\bar{\mu} > 0$ are the Lamé coefficients of steel; $\boldsymbol{\varepsilon}(u) = \frac{1}{2}(\nabla u + \nabla u^T)$ is the strain tensor; $A_1(a, m, \theta)\boldsymbol{I}$ models the thermal strain, $\boldsymbol{I}$ being the $3 \times 3$ unity matrix, whereas

$A_1(a,m,\theta)$ is defined as

$$A_1(a,m,\theta) = q_a a(\theta-\theta_a) + q_m m(\theta-\theta_m) + q_r(1-a-m)(\theta-\theta_r),$$

and in its turn $q_a$, $q_m$ and $q_r$ are the thermal expansion coefficients of the phase fractions $a$, $m$ and $r$, respectively, and $\theta_a$, $\theta_m$ and $\theta_r$ are reference temperatures (notice that during the heating stage is $m=0$); $\int_0^t \gamma(a,m,a_t,m_t,\theta)\boldsymbol{S}\,\mathrm{d}\tau$ gives the model, through the function $\gamma$, of the transformation induced plasticity strain tensor, where $\boldsymbol{S} = \boldsymbol{\sigma} - \frac{1}{3}\operatorname{tr}\sigma\boldsymbol{I}$ is the deviator of $\sigma$, that is the trace free part of the stress tensor; $\Gamma_0$ and $\Gamma_1$ is a partition of $\partial\Omega^{\mathrm{s}}$, both surfaces being smooth enough; $n$ is the unit outer normal vector to the boundary $\Gamma_1$; the functions $\tau_a(\theta)$, $a_{\mathrm{eq}}(\theta)$ are given from experimental data fitting the corresponding CCT diagram (see Figure 4), and $\mathcal{H}$ is the Heaviside function; $\kappa(\theta)$ is the thermal conductivity; the functions in (2.13) are given as follows

$$\alpha(\theta,a,m,\boldsymbol{\sigma}) = \rho c_\varepsilon - 9\bar{\kappa}q(a,m)^2\theta - q(a,m)\operatorname{tr}\boldsymbol{\sigma},$$

where $\rho$ and $c_\varepsilon$ are the steel density and the specific heat capacity at constant strain, respectively, $\bar{\kappa} = \frac{1}{3}(3\bar{\lambda}+2\bar{\mu})$ is the bulk modulus, and $q(a,m)$ is defined as

$$q(a,m) = q_a a + q_m m + (1-a-m)q_r;$$

$$A_2(a_t,m_t,\theta) = q_a a_t(\theta-\theta_a) + q_m m_t(\theta-\theta_m) - q_r(a_t+m_t)(\theta-\theta_r).$$

Finally, $L_a > 0$ is the latent heat related to the austenite phase fraction. Notice that, in a more general case $\rho$, $c_\varepsilon$ and $L_a$ may depend on $a$, $m$ and/or $\theta$.

Equations (2.1) and (2.4) derive from Maxwell's equations. In [9], it is assumed the Coulomb gauge condition for the magnetic vector potential, namely, $\nabla\cdot\boldsymbol{\mathcal{A}} = 0$. Here, we do not impose this condition since this makes appear an undesired pressure gradient in the equation for $\boldsymbol{\mathcal{A}}$. In its turn, we include a penalty term in this equation of the form $-\delta\nabla(\nabla\cdot\boldsymbol{\mathcal{A}})$. In doing so, both the theoretical analysis and the numerical simulations are simplified.

Equation (2.7) is a quasistatic balance law of momentum and (2.7) is Hooke's law. The transformation to austenite from the initial phase $r(0)=1$ is described in (2.11).

Finally, equation (2.13) derives from the balance law of internal energy. As it has been pointed out above, Joule's heating is the main responsible in heat production. Since

$\gamma(a, m, a_t, m_t, \theta)|\boldsymbol{S}|^2 \geq 0$, the contribution of the transformation induced plasticity to the energy balance is also a production term. On the other hand, during the heating stage we have $a_t \geq 0$ so that $-\rho L_a a_t \leq 0$. This means that the transformation to austenite absorbs energy, which is released during the cooling stage.

## The cooling model

The heating process ends, the high frequency current passing through the coil is switched-off and aqua-quenching begins. The quenching is just modeled via the Robin boundary condition given in (2.25).

We put $a_{T_\mathrm{h}} = a(T_\mathrm{h})$, that is, $a_{T_\mathrm{h}}$ is the austenite phase fraction distribution at the final heating instant $T_\mathrm{h}$ obtained from (2.11). In the same way, we define $\theta_{T_\mathrm{h}} = \theta(T_\mathrm{h})$. Obviously, these functions will be taken as the initial phase fraction distribution and temperature, respectively, in the cooling model. Here we use the Koistinen-Marburger model ([11, 13]) for the description of the transformation to martensite from austenite.

The cooling model reads as follows:

$$-\nabla \cdot \boldsymbol{\sigma} = F \quad \text{in } \Omega^\mathrm{s} \times (T_\mathrm{h}, T_\mathrm{c}), \tag{2.16}$$

$$\boldsymbol{\sigma} = \boldsymbol{K}\left(\boldsymbol{\varepsilon}(u) - A_1(a, m, \theta)\boldsymbol{I} - \int_0^t \gamma(a, m, a_t, m_t, \theta)\boldsymbol{S}\,\mathrm{d}\tau\right), \tag{2.17}$$

$$u = 0 \quad \text{on } \Gamma_0 \times (T_\mathrm{h}, T_\mathrm{c}), \tag{2.18}$$

$$\boldsymbol{\sigma}\, n = 0 \quad \text{on } \Gamma_1 \times (T_\mathrm{h}, T_\mathrm{c}), \tag{2.19}$$

$$a_t = \frac{1}{\tau_a(\theta)}(a_\mathrm{eq}(\theta) - a)\mathcal{H}(\theta - A_s) \quad \text{in } \Omega^\mathrm{s} \times (T_\mathrm{h}, T_\mathrm{c}), \tag{2.20}$$

$$a(T_\mathrm{h}) = a_{T_\mathrm{h}} \quad \text{in } \Omega^\mathrm{s}, \tag{2.21}$$

$$m_t = c_m(1 - m)\mathcal{H}(-\theta_t)\mathcal{H}(M_s - \theta) \quad \text{in } \Omega^\mathrm{s} \times (T_\mathrm{h}, T_\mathrm{c}), \tag{2.22}$$

$$m(T_\mathrm{h}) = 0 \quad \text{in } \Omega^\mathrm{s}, \tag{2.23}$$

$$\begin{aligned}\alpha(\theta, a, m, \boldsymbol{\sigma})\theta_t - \nabla \cdot (\kappa(\theta)\nabla\theta) + 3\bar{\kappa}q(a, m)\theta\,(\nabla \cdot u_t - 3A_2(a_t, m_t, \theta)) = \\ = -\rho L_a a_t + \rho L_m m_t + A_2(a_t, m_t, \theta)\,\mathrm{tr}\,\boldsymbol{\sigma} + \gamma(a, m, a_t, m_t, \theta)|\boldsymbol{S}|^2 \quad \text{in } \Omega \times (T_\mathrm{h}, T_\mathrm{c}),\end{aligned} \tag{2.24}$$

$$\frac{\partial\theta}{\partial n} = \beta(x, t)(\theta - \theta_\mathrm{e}) \quad \text{on } \partial\Omega \times (T_\mathrm{h}, T_\mathrm{c}), \tag{2.25}$$

$$\theta(T_\mathrm{h}) = \theta_{T_\mathrm{h}} \quad \text{in } \Omega. \tag{2.26}$$

In (2.22) $c_m > 0$ is a constant value. Also, in (2.24), $L_m > 0$ is the latent heat related to the martensite phase fraction. The function $\beta(x,t)$ in (2.25) is a heat transfer coefficient and is given by

$$\beta(x,t) = \begin{cases} 0 & \text{on } \partial\Omega \cap \partial\Omega^{\mathrm{c}}, \\ \beta_0(t) & \text{on } \partial\Omega \cap \partial\Omega^{\mathrm{s}}. \end{cases}$$

where $\beta_0(t) > 0$ (usually taken to be constant). Finally, $\theta_{\mathrm{e}}$ is the temperature of the quenchant.

The mathematical analysis of a system similar to (2.16)-(2.26) can be seen in [3]. In this reference, an existence result is shown assuming that the data are smooth enough and $T_{\mathrm{c}} - T_{\mathrm{h}}$ is sufficiently small.

## 3 The harmonic regime

We focus our attention on the heating induction-conduction process. Electromagnetic fields generated by high frequency currents are sinusoidal in time. Consequently, both the electric potential, $\phi$, and the magnetic potential field, $\boldsymbol{\mathcal{A}}$, take the form ([1, 2, 14, 15]) $\mathcal{M}(x,t) = \mathrm{Re}\,[e^{i\omega t}M(x)]$, where $M$ is a complex-valued function or vector field, and $\omega = 2\pi f$ is the angular frequency, $f$ being the electric current frequency. In general, $M$ also depends on $t$, but at a time scale much greater than $1/\omega$. In this way, we may introduce the complex-valued fields $\varphi$, $\boldsymbol{A}$ and $\boldsymbol{j}$ as

$$\phi = \mathrm{Re}[e^{i\omega t}\varphi(x,t)], \quad \boldsymbol{\mathcal{A}} = \mathrm{Re}[e^{i\omega t}\boldsymbol{A}(x,t)], \quad j_S = \mathrm{Re}[e^{i\omega t}\boldsymbol{j}(x)]. \tag{3.1}$$

As far as the numerical simulation of a system like (2.1)-(2.15) is concerned, the introduction of the new variables $\varphi$ and $\boldsymbol{A}$ is quite convenient since the time scale describing the evolution of both $\varphi$ and $\boldsymbol{A}$ is much smaller than that of the temperature $\theta$. In the case of steel heat treating, $f$ is about 80 KHz.

Rewriting the original system (2.1)-(2.15) in terms of the new complex-valued variables, $\varphi$ and $\boldsymbol{A}$, neglecting the term $\boldsymbol{A}_t$, we obtain the so-called harmonic regime. Furthermore, in the energy equation, the expression $|\boldsymbol{\mathcal{A}}_t + \nabla\phi|^2$ is substituted by its mean value measured over a time period $[t, t+\omega]$:

$$\frac{1}{\omega}\int_t^{t+\omega} |\boldsymbol{\mathcal{A}}_t + \nabla\phi|^2 \simeq \frac{1}{2}|i\omega\boldsymbol{A} + \nabla\varphi|^2. \tag{3.2}$$

In this way, the effective Joule's heating takes the form $\frac{1}{2}b(\theta)|i\omega\boldsymbol{A}+\nabla\varphi|^2$. Notice that if both $\boldsymbol{A}$ and $\varphi$ are time independent, then the expression (3.2) is in fact an equality and the right hand side does not depend on the integration interval $[t,t+\omega]$.

The equations in the harmonic regime are the following:

$$\nabla\cdot(b(\theta)\nabla\varphi)=0 \quad \text{in } \Omega_{T_\mathrm{h}}=\Omega\times(0,T_\mathrm{h}), \tag{3.3}$$

$$\frac{\partial\varphi}{\partial n}=0 \quad \text{on } \partial\Omega\times(0,T_\mathrm{h}), \tag{3.4}$$

$$\left[b(\theta)\frac{\partial\varphi}{\partial n}\right]_\Gamma=\boldsymbol{j} \quad \text{on } \Gamma\times(0,T_\mathrm{h}), \tag{3.5}$$

$$b_0(\theta)i\omega\boldsymbol{A}+\nabla\times\left(\frac{1}{\mu}\nabla\times\boldsymbol{A}\right)-\delta\nabla(\nabla\cdot\boldsymbol{A})=-b_0(\theta)\nabla\varphi \quad \text{in } D\times(0,T_\mathrm{h}), \tag{3.6}$$

$$\boldsymbol{A}=0 \quad \text{on } \partial D\times(0,T_\mathrm{h}), \tag{3.7}$$

$$-\nabla\cdot\boldsymbol{\sigma}=F \quad \text{in } \Omega^\mathrm{s}\times(0,T_\mathrm{h}), \tag{3.8}$$

$$\boldsymbol{\sigma}=\boldsymbol{K}\left(\boldsymbol{\varepsilon}(u)-A_1(a,m,\theta)\boldsymbol{I}-\int_0^t\gamma(a,m,a_t,m_t,\theta)\boldsymbol{S}\,\mathrm{d}\tau\right), \tag{3.9}$$

$$u=0 \quad \text{on } \Gamma_0\times(0,T_\mathrm{h}), \tag{3.10}$$

$$\boldsymbol{\sigma}\,n=0 \quad \text{on } \Gamma_1\times(0,T_\mathrm{h}), \tag{3.11}$$

$$a_t=\frac{1}{\tau_a(\theta)}(a_\mathrm{eq}(\theta)-a)\mathcal{H}(\theta-A_s) \quad \text{in } \Omega^\mathrm{s}\times(0,T_\mathrm{h}), \tag{3.12}$$

$$a(0)=0 \quad \text{in } \Omega^\mathrm{s}, \tag{3.13}$$

$$\begin{aligned}&\alpha(\theta,a,m,\boldsymbol{\sigma})\theta_t-\nabla\cdot(\kappa(\theta)\nabla\theta)+3\bar{\kappa}q(a,m)\theta\,(\nabla\cdot u_t-3A_2(a_t,m_t,\theta))=\\&=\frac{1}{2}b(\theta)|i\omega\boldsymbol{A}+\nabla\varphi|^2-\rho L_a a_t+A_2(a_t,m_t,\theta)\,\mathrm{tr}\,\boldsymbol{\sigma}+\gamma(a,m,a_t,m_t,\theta)|\boldsymbol{S}|^2 \quad \text{in } \Omega_{T_\mathrm{h}},\end{aligned} \tag{3.14}$$

$$\frac{\partial\theta}{\partial n}=0 \quad \text{on } \partial\Omega\times(0,T_\mathrm{h}), \tag{3.15}$$

$$\theta(0)=\theta_0 \quad \text{in } \Omega. \tag{3.16}$$

An existence result for a simpler version of the system (3.3)-(3.16), without taking into account mechanical effects, (that is, $\boldsymbol{\sigma}=0$ and $u=0$) has been announced in [6].

# 4 Numerical simulation

Using the Freefem++ package ([8]), we have performed some numerical simulations for the approximation of the solution to the systems (3.3)-(3.16) and (2.16)-(2.26). In these simulations we do not consider mechanical effects ($\boldsymbol{\sigma} = 0$, $u = 0$) and we are interested in the evolution of the temperature, the austenization process and the martensite transformation ([5]). We want to describe the hardening treatment of a car steering rack during the heating-cooling process. The goal is to produce martensite along the tooth line together with a thin layer in its neighborhood inside the steel workpiece.

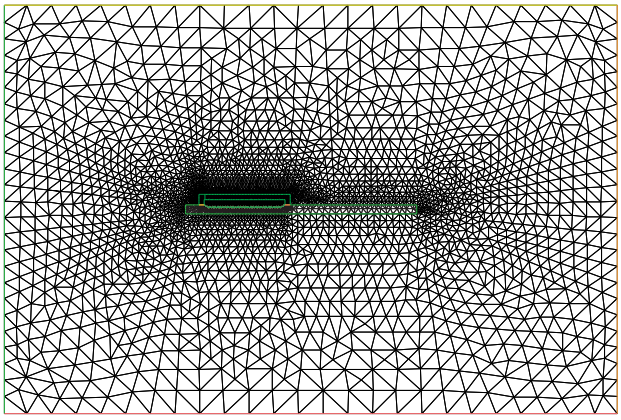

Figure 6: Domain triangulation. The mesh contains 61790 triangles and 30946 vertices.

Figure 5 shows the open sets $D$, $\Omega = \Omega^s \cup \Omega^c \cup S$ and the inferface $\Gamma$ which intervene in the setting of the problem. The workpiece contains a toothed part to be hardened by means of the heating-cooling process described above. It is made of a hypoeutectoid steel. The open set $D \setminus \bar{\Omega}$ is air. The magnetic permeability $\mu$ in (3.6) is then given by

$$\mu(x) = \begin{cases} \mu_0 & \text{if } x \in D \setminus \bar{\Omega}, \\ 0.99995\mu_0 & \text{if } x \in \Omega^c, \\ 2.24 \times 10^3 \mu_0 & \text{if } x \in \Omega^s, \end{cases}$$

where $\mu_0 = 4\pi \times 10^{-7}$ (N/A$^2$) is the magnetic constant (vacuum permeability).

The martensite phase can only derive from the austenite phase. Thus we need to transform first the critical part to be hardened (the tooth line) into austenite. For our

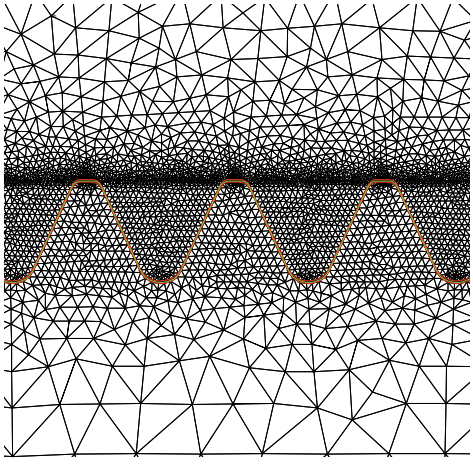

Figure 7: Domain triangulation. Element density near three teeth.

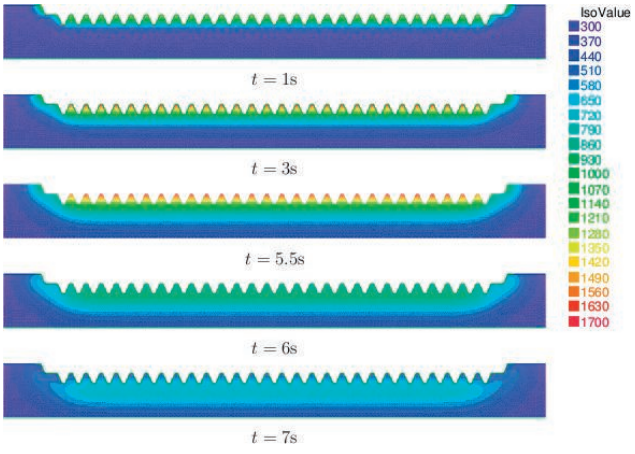


Figure 8: Temperature evolution at instants $t = 1$, $t = 3$, $t = 5.5$ (end of the heating stage, aqua-quenching begins), $t = 6$ and $t = 7$ seconds, respectively. At $t = 5.5$ s the temperature along the tooth part has reached the austenization level in this part of the rack. The temperature is measured in Kelvin degrees.

hypoeutectoid steel, austenite only exists in a temperature range close to the interval $[1050, 1670]$ (in °K). During the first stage, the workpiece is heated up by conduction and

induction (Joule's heating) which renders the tooth line to the desired temperature. In order to transform the austenite into martensite, we must cool it down at a very high rate. This second stage is accomplished by spraying water over the workpiece.

In this simulation, the final time of the heating process is $T_{\rm h} = 5.5$ seconds and the cooling process extends also for 5.5 seconds, that is $T_{\rm c} = 11$.

We have used the finite elements method for the space approximation and a Crank-Nicolson scheme for the time discretization. Figures 6 and 7 show the triangulation of $D$ in our numerical simulations. We have used $P_2$-Lagrange approximation for $\varphi$, $\boldsymbol{A}$ and $\theta$ and $P_1$ for $a$ and $m$.

In Figure 8 we can see the temperature distribution of the rack along the tooth line at different instants of the the heating-cooling process. The initial temperature is $\theta_0 = 300$°K. At $t = 5.5$ the heating process ends and the computed temperature shows that the temperature along the rack tooth line lies in the interval $[1050, 1670]$ (°K).

Figure 10 shows the austenization along the tooth line at the end of the heating process $T = 5.5$ seconds.

Figure 11 shows the final distribution of martensite from austenite along the rack tooth line through the cooling stage $t = 11$ seconds. We have good agreement versus the experimental results obtained in the industrial process.

## Acknowledgements

This research was partially supported by Ministerio de Educación y Ciencia under grant MTM2006-04436 with the participation of FEDER, and Consejería de Educación y Ciencia de la Junta de Andalucía, research group FQM–315.

## References

[1] A. Bermúdez, J. Bullón, F. Pena and P. Salgado, *A numerical method for transient simulation of metallurgical compound electrodes*, Finite Elem. Anal. Des., **39**, 283-299, 2003.

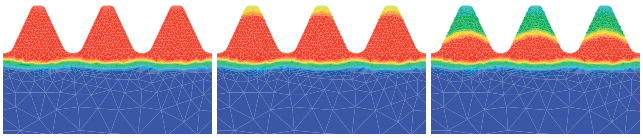

Austenite: $t = 5.5$s (left), $t = 6.5$s (center) and $t = 7$s (right)

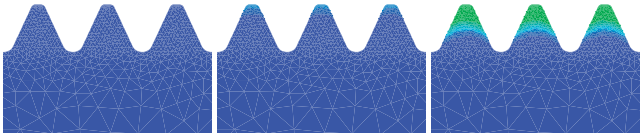

Martensite: $t = 5.5$s (left), $t = 6.5$s (center) and $t = 7$s (right)

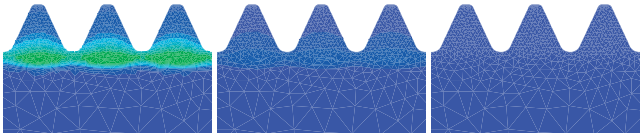

Austenite: $t = 8$s (left), $t = 9$s (center) and $t = 11$s (right)

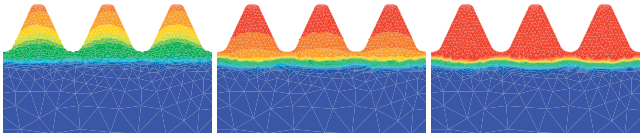

Martensite: $t = 8$s (left), $t = 9$s (center) and $t = 11$s (right)

Figure 9: Transformation of the martensite phase fraction from austenite during the aqua-quenching at time instants t=5.5, 6.5, 7, 8, 9, and 11 seconds, respectively. Blue corresponds to 0% while red is 100%. We observe that martensite starts to appear, approximatively, one second after the beginning of the cooling stage. At the final instant, all the amount of austenite has been transformed into martensite.

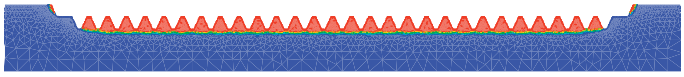

Figure 10: Heating process. Austenite at $t = 5.5$ along the rack tooth line.

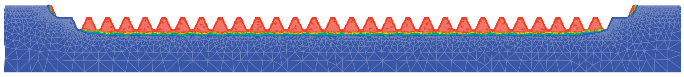

Figure 11: Cooling process. Martensite transformation at the final stage of the cooling process $t = 11$ seconds.

[2] A. Bermúdez, D. Gómez, M. C. Muñiz and P. Salgado, *Transient numerical simulation of a thermoelectrical problem in cylindrical induction heating furnaces*, Adv. Comput. Math., **26**, 39-62, 2007.

[3] K. Chełminski, D. Hömberg and D. Kern, *On a thermomechanical model of phase transitions in steel*, WIAS preprint, **1125**, Berlin 2007.

[4] J. R. Davis *et al. ASM Handbook: Heat Treating*, vol. **4**, ASM International, USA, 2007.

[5] J. M. Díaz Moreno, C. García Vázquez, M. T. González Montesinos and F. Ortegón Gallego, *Numerical simulation of a Induction-Conduction Model Arising in Steel Hardening model arising in steel hardening*, Lecture Notes in Engineering and Computer Science, World Congress on Engineering 2009, Volume II, July 2009, 1251–1255.

[6] J. M. Díaz Moreno, C. García Vázquez, M. T. González Montesinos and F. Ortegón Gallego, *Analysis and numerical simulation of an induction-conduction model arising in steel heat treating*, Proceedings of the 10th International Conference on Computational and Mathematical Methods in Science and Engineering, CMMSE 2010.

[7] J. Fuhrmann, D. Hömberg and M. Uhle, *Numerical simulation of induction hardening of steel,* COMPEL, **18**, No. 3, 482–493, 1999.

[8] F. Hecht, O. Pironneau, A. Le Hyaric, K. Ohtsuda, *Freefem++*, `http://www.freefem.org/ff++`.

[9] D. Hömberg, *A mathematical model for induction hardening including mechanical effects*, Nonlinear Analysis: Real World Applications, **5**, 55–90, 2004.

[10] D. Hömberg and W. Weiss, *PID control of laser surface hardening of steel*, IEEE Transactions on Control Systems Technology, **14**, No. 5, 896–904, 2006.

[11] D. P. Koistinen, R. E. Marburger, *A general equation prescribing the extent of the austenite-martensite transformation in pure iron-carbon alloys and plain carbon steels*, Acta Met., 7 (1959), 59–60.

[12] G. Krauss, *Steels: Heat Treatment and Processing Principles*, ASM International, USA, 2000.

[13] J. B. Leblond and J. Devaux, *A new kinetic model for anisothermal metallurgical transformations in steels including effect of austenite grain size*, Acta metall., **32**, No. 1, 137–146, 1984.

[14] F. J. Pena Brage, *Contribución al modelado matemático de algunos problemas en la metalurgia del silicio*, Ph. thesis, Universidade de Santiago de Compostela, 2003.

[15] H. M. Yin, *Regularity of weak solution to Maxwell's equations and applications to microwave heating*, J. Differential Equations, **200**, 137-161, 2004.